

Ubp6 deubiquitinase controls conformational dynamics and substrate degradation of the 26S proteasome

Charlene Bashore¹, Corey M Dambacher², Ellen A Goodall¹, Mary E Matyskiela^{1,4}, Gabriel C Lander² & Andreas Martin^{1,3}

Substrates are targeted for proteasomal degradation through the attachment of ubiquitin chains that need to be removed by proteasomal deubiquitinases before substrate processing. In budding yeast, the deubiquitinase Ubp6 trims ubiquitin chains and affects substrate processing by the proteasome, but the underlying mechanisms and the location of Ubp6 within the holoenzyme have been elusive. Here we show that Ubp6 activity strongly responds to interactions with the base ATPase and the conformational state of the proteasome. Electron microscopy analyses reveal that ubiquitin-bound Ubp6 contacts the N ring and AAA+ ring of the ATPase hexamer and is in proximity to the deubiquitinase Rpn11. Ubiquitin-bound Ubp6 inhibits substrate deubiquitination by Rpn11, stabilizes the substrate-engaged conformation of the proteasome and allosterically interferes with the engagement of a subsequent substrate. Ubp6 may thus act as a ubiquitin-dependent ‘timer’ to coordinate individual processing steps at the proteasome and modulate substrate degradation.

Cell survival fundamentally depends on protein degradation, which in eukaryotes is carried out to a large extent by the ubiquitin-proteasome system (UPS)^{1,2}. Cells must maintain the proteome and degrade misfolded or damaged polypeptides. Degradation of regulatory and signaling proteins mediates numerous vital processes including transcription and cell division³. The final destination in the UPS, the essential 26S proteasome, is a compartmental protease of the AAA+ family that mechanically unfolds and degrades protein substrates in an ATP-dependent manner. Most proteasomal substrates are marked for degradation and targeted to the proteasome by the enzymatic attachment of ubiquitin chains, which must be removed by intrinsic deubiquitinases (DUBs) at the proteasome to allow efficient turnover^{4,5}.

The *Saccharomyces cerevisiae* 26S proteasome consists of at least 34 different subunits that assemble into a 2.5-MDa complex. At the center of the holoenzyme is the barrel-shaped 20S core particle (CP), which sequesters the proteolytic active sites⁶. Access to the degradation chamber is controlled by the 19S regulatory particle (RP), which caps one or both ends of the 20S peptidase and can be further separated into base and lid subcomplexes. The base contains three non-ATPase subunits (Rpn1, Rpn2 and Rpn13); it also contains six distinct AAA+ ATPases (Rpt1–Rpt6), which form a heterohexameric ring with a central processing pore and constitute the unfoldase motor of the proteasome. ATP hydrolysis in the AAA+ domains of these ATPases is thought to drive conformational changes and to propel movements of conserved pore loops to mechanically pull on substrate polypeptides and translocate them through the central channel into the peptidase^{7–9}. Each Rpt subunit also contains an N-terminal OB-fold domain, which assembles into a distinct N ring above the AAA+ domain ring in

the hexamer. The lid subcomplex acts as a scaffold bound to one side of the base and contains the metalloprotease Rpn11, which is the essential deubiquitinase of the proteasome^{4,5}. The base and lid subcomplexes must work together to recognize, process and ultimately deliver substrates to the proteolytic core particle for cleavage into small peptides. Substrate proteins modified with ubiquitin chains of different linkage types—particularly K11 and K48 linkages, but also K63 linkages *in vitro*^{10–12}—are tethered to the proteasome by interacting with the intrinsic receptors Rpn10 and Rpn13 or with transiently bound shuttle receptors^{13–17}. Subsequently, the ATPase ring of the base engages an unstructured initiation region of the substrate and uses ATP hydrolysis to mechanically unfold and translocate the polypeptide. Concomitant with substrate translocation is the removal of ubiquitin modifications by the DUB Rpn11, which is localized above the entrance to the central pore of the base^{18,19}.

Substrate degradation involves multiple conformational states of the proteasome regulatory particle. In the substrate-free state, the AAA+ domains of the Rpts adopt a steep spiral-staircase arrangement that may facilitate substrate engagement²⁰. Engagement induces the transition to the actively translocating state. This state is characterized by a more planar spiral-staircase arrangement of the Rpts as well as by a coaxial alignment of the N ring and AAA+ ring with the peptidase, both of which create a continuous central channel for substrate translocation into the degradation chamber^{21,22}. Furthermore, during this conformational change of the regulatory particle, Rpn11 shifts to a central position above the entrance to the pore, where it is ideally placed to scan for and remove ubiquitins from substrates as they are translocated by the base ATPases. Thus, we surmise that for every

¹Department of Molecular and Cell Biology, University of California, Berkeley, Berkeley, California, USA. ²Department of Integrative Structural and Computational Biology, Scripps Research Institute, La Jolla, California, USA. ³California Institute for Quantitative Biosciences, University of California, Berkeley, Berkeley, California, USA. ⁴Present address: Celgene Corporation, San Diego, California, USA. Correspondence should be addressed to A.M. (a.martin@berkeley.edu).

Received 4 May; accepted 27 July; published online 24 August 2015; doi:10.1038/nsmb.3075

substrate turnover, the proteasome transitions from a substrate-free, engagement-competent state to an engaged state that facilitates processive translocation, unfolding and deubiquitination. The proteasome must switch back to the substrate-free conformation before the engagement of a subsequent substrate.

In addition to containing Rpn11, the 26S proteasome from *S. cerevisiae* contains another stably associated deubiquitinase, Ubp6, which shows high sequence and structural conservation with its human homolog, Usp14 (ref. 23). This 60-kDa ubiquitin-specific protease (USP) uses an active site cysteine to cleave the isopeptide bonds within ubiquitin chains. Ubp6 is known to interact with Rpn1 of the base, but efforts to localize either Ubp6 or Usp14 in the context of the proteasome have failed^{24,25}. Moreover, Ubp6 has been shown to catalytically and noncatalytically affect the rates of proteasomal degradation. Ubp6 interferes with the critical substrate deubiquitination by Rpn11, stimulates 20S gate opening and thus increases access to the degradation chamber and enhances the rates of ATP hydrolysis^{26–29}. However, the mechanisms by which Ubp6 modulates the activities of the proteasome remain poorly understood.

Depletion of Ubp6 or Usp14 activity has dramatic consequences *in vivo*. Loss of Ubp6 function, for example, increases aneuploidy tolerance in yeast, presumably owing to an elevated proteasome capacity for turning over higher protein levels, and pharmacological inhibition of Usp14 in human cells has been shown to stimulate proteasome activity^{29–31}. In the hippocampus, loss of Usp14 binding to the proteasome results in higher degradation rates that interfere with presynaptic formation, which can be rescued by overexpression of a catalytically inactive mutant³². Thus, both the catalytic and noncatalytic effects of Ubp6 on proteasome activity have important implications in cellular protein turnover. Understanding the interactions of Ubp6 with the proteasome in structural and mechanistic detail is therefore expected to provide important new insights into the role of this deubiquitinase in maintaining the proteome.

In this study, we used biochemical and structural approaches on reconstituted proteasome complexes to investigate the nature of the Ubp6 interaction. We found that the deubiquitination activity of Ubp6 depends on binding to the base ATPase and responds to the conformational state of the proteasome. By engineering a substrate-recruitment system independent of polyubiquitin, we were able to separate catalytic and noncatalytic effects of Ubp6 on proteasomal activities. We localized Ubp6 by EM and show that it contacts both the N ring and the AAA+ ring of the base in its substrate-engaged conformation, thus positioning the deubiquitinase so that it directly faces Rpn11. The position of Ubp6 is consistent with our biochemical findings that the ubiquitin-bound deubiquitinase strongly inhibits Rpn11 deubiquitination activity, stabilizes the translocating conformation of the holoenzyme and prevents engagement of subsequent substrates.

RESULTS

Ubp6 activity responds to proteasome conformational states

The deubiquitination activity of Ubp6 has been shown to dramatically increase upon binding to the 26S proteasome^{24,26,29}. To assess the mechanisms of this activation, we measured Ubp6 deubiquitination in the presence of purified proteasome subcomplexes²⁰ and 4-aminomethylcoumarin-fused ubiquitin (Ub-AMC), a substrate that fluoresces upon cleavage (Fig. 1). In spite of its known interaction with Ubp6, Rpn1 alone failed to stimulate Ubp6 activity, whereas purified base or holoenzyme induced a 300-fold increase in deubiquitination. Thus, full activation of Ubp6 requires contacts with other base subunits in addition to Rpn1 (Fig. 1a).

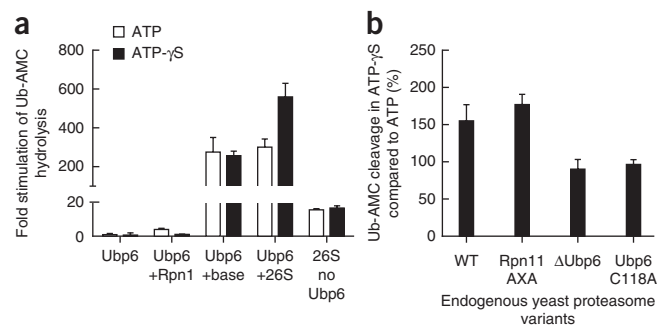


Figure 1 Ubp6 deubiquitination activity responds to the conformational state of the proteasome. Ub-AMC cleavage activity of Ubp6 was measured in response to interactions with the proteasomes as holoenzyme or isolated subcomplexes. (a) Deubiquitination assays with proteasomes reconstituted with heterologously expressed base subcomplex purified from *Escherichia coli* as well as core and lid subcomplexes purified from yeast, in the presence of ATP or the nonhydrolyzable ATP-γS, which induces the engaged state of the proteasome. (b) Deubiquitination assays with proteasomes purified from yeast strains with wild-type, deleted or inactive (C118A) Ubp6, or with wild-type Ubp6 and an inactive Rpn11 (AXA). Shown are the relative activities in the presence of ATP-γS compared to ATP. Data are means and s.e.m. of three independent experiments. Compiled experimental data are shown in **Supplementary Data Set 2**.

Interestingly, Ubp6 deubiquitination activity also responds to the conformational state of the proteasome. ATP-γS has previously been shown to invoke a conformation similar to that of the substrate-engaged state^{21,22} (**Supplementary Fig. 1**). We therefore reconstituted the proteasome in the presence of ATP-γS and observed a 1.9-fold increase in Ubp6 deubiquitination activity compared to that of the ATP-bound, substrate-free state of the proteasome (Fig. 1a). Importantly, we also found this Ubp6 stimulation for endogenous 26S holoenzyme purified from yeast (Fig. 1b), a result suggesting that the deubiquitinase indeed responds to an ATP-γS-induced conformational change and not to an alternative assembly state during *in vitro* reconstitution. Proteasomes lacking Ubp6 or containing Ubp6 with a mutated active site cysteine (C118A) did not show this ATP-γS-dependent stimulation of deubiquitination, whereas the effect was still present for proteasomes with the catalytically inactive⁴ Rpn11 AXA mutant (Fig. 1b). These results indicate that Ubp6, not Rpn11, is responsible for the stimulated deubiquitination activity in response to the engaged state of the proteasome.

Ubp6 allostery is connected to substrate engagement

Previous studies have shown that polyubiquitin-bound Ubp6 stimulates the ATPase rate of the proteasome²⁸. This observation, together with our findings that ATP- and ATP-γS-bound proteasomes differentially stimulate the deubiquitination activity of Ubp6, suggest that Ubp6 may have a role in the conformational dynamics of the holoenzyme. The function of Ubp6 in ubiquitin processing during substrate degradation, however, complicates a detailed analysis of such potential allosteric effects. To deliver substrates to the proteasome in a ubiquitin-independent manner, we therefore developed an artificial recruitment system by fusing a permuted single-chain variant of the dimeric substrate adaptor SspB₂ to the N terminus of the ATPase subunit Rpt2 (Fig. 2a). In bacteria, SspB₂ recruits substrates to the AAA+ protease ClpXP by recognizing a portion of the 11-amino acid ssrA tag³³. Including this ssrA tag in our model substrates enables their ubiquitin-independent targeting to SspB₂-fused reconstituted proteasomes (Fig. 2b), which are still capable of degrading

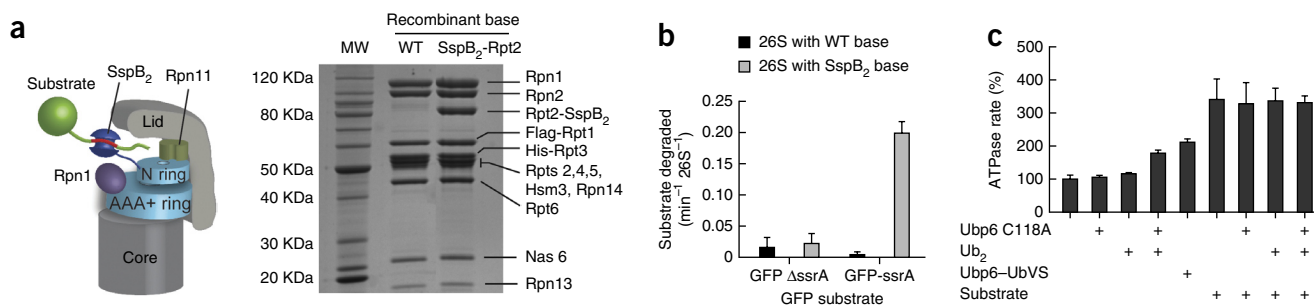


Figure 2 Ubp6 allostery is connected to substrate engagement. To separate ubiquitin processing from substrate engagement and translocation, we designed a ubiquitin-independent recruitment system by fusing a linked permutant of the bacterial dimeric substrate adaptor SspB₂ to Rpt2 of the base. **(a)** Left, schematic of a SspB₂-fused proteasome recruiting an ssrA-tagged substrate. Right, SDS-PAGE of *E. coli*-expressed base subcomplex with either wild-type (WT) or SspB₂-fused Rpt2. MW, molecular-weight marker. **(b)** Degradation of a GFP model substrate containing the ssrA recognition motif, measured in proteasomes reconstituted with either wild-type or SspB₂-fused base complexes. **(c)** Stimulation of ATPase rate of SspB₂-fused proteasomes by ubiquitin-bound Ubp6 (Ubp6 C118A with diubiquitin or ubiquitin vinyl sulfone–fused Ubp6 (Ubp6–UbVS)) and substrate translocation. Data in **b** and **c** are means and s.e.m. of three technical replicates. Compiled experimental data are shown in **Supplementary Data Set 2**.

ubiquitinated substrates (**Supplementary Fig. 2a**). The SspB₂-fused proteasomes allowed us to compare how ubiquitin binding to Ubp6 and substrate engagement by the AAA+ ring stimulate ATP hydrolysis and to assess whether these processes affect the same or distinct conformations of the proteasome.

To enforce a ubiquitin-bound state of Ubp6, we used the catalytically inactive C118A mutant and incubated it with purified K48-linked ubiquitin dimers³⁴. Ubp6 C118A led to a 1.8-fold increase of proteasome ATPase activity only in the presence of diubiquitin (**Fig. 2c**); we also observed comparable effects for ATPase stimulation of the isolated base subcomplex (**Supplementary Fig. 2b**). The ATPase response of SspB₂-fused proteasomes to ubiquitin-bound Ubp6 C118A strongly resembled the behavior of wild-type proteasomes (**Supplementary Fig. 2c**), thus confirming that the SspB₂-fusion construct is well suited to separate ubiquitin-related processes from other aspects of substrate degradation. In addition, we covalently modified wild-type Ubp6's active site cysteine with ubiquitin vinyl sulfone (UbVS)³⁵. The resultant Ubp6–UbVS stimulated the proteasome ATPase activity similarly to Ubp6 C118A in the presence of ubiquitin dimers (**Fig. 2c**), thus confirming that it is indeed the ubiquitin-bound state of Ubp6 that is responsible for the observed ATPase stimulation.

To analyze the substrate-induced stimulation of ATP hydrolysis, we used the SspB₂-fused proteasomes in combination with an ssrA-tagged, permanently unfolded model protein that can be engaged and rapidly translocated without the extra burden of protein unfolding. Processing of this substrate caused a 3.3-fold increase in the ATPase rate of reconstituted proteasomes (**Fig. 2c**). Importantly, the addition of Ubp6 C118A and diubiquitin did not lead to a further increase, thus suggesting that substrate- and ubiquitin-bound Ubp6 stimulate ATP hydrolysis by inducing or stabilizing a similar proteasome state, albeit to a different extent. Our previous structural comparison between substrate-free and substrate-engaged proteasomes suggested that the ATPase stimulation upon substrate engagement is caused by a switching of the AAA+ ring from a steep spiral-staircase conformation to a more planar conformation with uniform Rpt-subunit interfaces²¹. Ubiquitin-bound Ubp6 may thus also partially induce or stabilize this engaged conformation of the Rpt ring, consistently with the observed reciprocal stimulation of Ubp6 deubiquitination activity by ATP-γS-bound proteasomes.

In support of this hypothesis, we found that substrate engagement and translocation also stimulate Ubp6 deubiquitination activity,

albeit not as strongly as trapping the base in a permanently engaged state with ATP-γS (**Supplementary Fig. 2d**). Unfortunately, the ATP-γS-bound state prevents substrate engagement and therefore made it impossible for us to assess whether the ATPase stimulation caused by substrate engagement and ATP-γS binding are indeed nonadditive, as expected on the basis of the strong similarities between the corresponding proteasome structures^{21,22}.

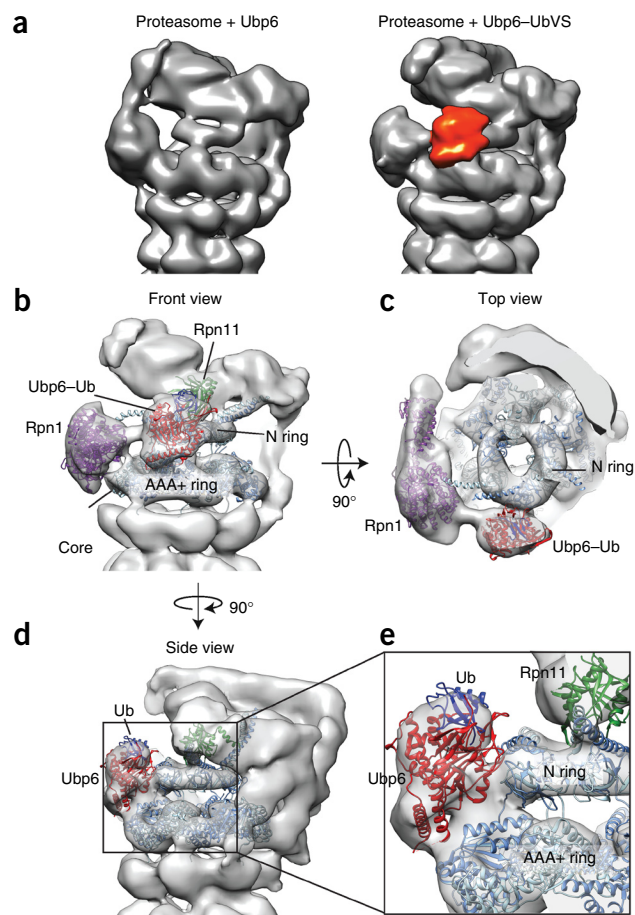
In summary, our data suggest that ubiquitin binding to Ubp6 and substrate engagement by the base result in the same proteasome state, which is marked by an increased ATPase rate and higher Ubp6 deubiquitination activity.

Ubp6 binds to the Rpt hexamer of the base

Previous biochemical studies have reported that Ubp6 is tethered to the proteasome through interactions of its N-terminal Ubl domain with the Rpn1 subunit of the base, yet attempts to visualize and localize Ubp6 bound to the proteasome have been unsuccessful^{18,19}. The Ubl and the catalytic USP domains of Ubp6 are connected by a flexible 23-amino acid linker²³, which may allow the deubiquitinase to sample a larger space around the regulatory particle for removal of ubiquitin chains docked on ubiquitin receptors Rpn10 or Rpn13. In addition to this mobile domain architecture of Ubp6, the high intrinsic flexibility of Rpn1, as indicated by consistently lower local resolutions in EM reconstructions^{18,19}, probably hampered the localization and visualization of proteasome-bound Ubp6.

Given the observed functional cross-talk between ubiquitin-bound Ubp6 and the base ATPase, we concluded that trapping Ubp6 in a ubiquitin-bound state might stabilize it on the proteasome for our EM structural studies. We therefore covalently modified Ubp6's active site cysteine with UbVS³⁵ and incubated the resultant Ubp6–UbVS with proteasomes in the presence of either ATP or ATP-γS. ATP-bound proteasomes with Ubp6–UbVS exhibited a large degree of conformational heterogeneity (**Supplementary Fig. 3**), which was clearly visible in the three-dimensional (3D) classification of the data set. Although we could distinguish multiple 3D structures representing a continuum of different conformational states of the regulatory particle (**Supplementary Fig. 3**), none of these reconstructed proteasomes in the presence of ATP contained sufficient particles to accurately localize the Ubp6 density. A 3D refinement of the combined data set shows the holoenzyme in the apo conformation with diminished density in certain areas of the lid and especially the base, a result probably indicating the presence of proteasome particles in the

Figure 3 Ubiquitin-bound Ubp6 interacts with the Rpt hexamer of the base. (a) 3D reconstructions of the proteasome holoenzyme in complex with ATP- γ S and ubiquitin-free (left) or permanently ubiquitin-bound Ubp6 (red; right). (b–e) PDB models of various RP subunits docked into the 3D electron density map obtained from negatively stained samples. Rpn1 is shown in purple (PDB 4CR4; chain Z)⁴⁵, Rpn11 in green (PDB 4O8X)⁴⁶ and the ATPase ring in blue (PDB 4CR4; chains H–M). The Ubp6–Ub homology model was docked into the corresponding density of the 22.3-Å-resolution map. Ubp6 is shown in red and ubiquitin in blue. PDB models for all Rpt proteins of the base are alternately colored in two different shades of blue. (b) Front view of the RP, showing connecting density between Rpn1 and the catalytic domain of Ubp6, which contacts the Rpt ring directly in front of Rpn11. (c) Top view of the RP, showing specific contacts between Ubp6 and the N-terminal domain of Rpt1. (d) Side view of the RP, showing Ubp6 bridging the N ring and the AAA+ ring in their coaxially stacked, engaged conformation; interaction of N-domain residues of Rpt1 with surface loops of Ubp6; and contacts between the AAA+ domain of Rpt1 and two C-terminal helices of Ubp6. (e) Zoomed-in view of d, highlighting the Ubp6-base interface and proximity to Rpn11. Ubp6 is ~20 Å away from Rpn11, and its bound ubiquitin is ~30 Å from the Rpn11 active site.



engaged or hybrid states (Supplementary Fig. 4). Previous reconstructions of the proteasome with ubiquitin-free Ubp6 did not show such heterogeneity, thus suggesting that ubiquitin-bound Ubp6 may partially induce alternate conformations. This would be consistent with its stimulation of base ATP hydrolysis. Importantly, we also detected additional weak density next to Rpn1, which contacts the ATPase hexamer and may correspond to a mobile Ubp6–UbVS.

In contrast to the ATP-bound complex, proteasomes incubated with ATP- γ S and Ubp6–UbVS exhibited less conformational heterogeneity and complete absence of the apo conformation, thus enabling 3D reconstructions of the holoenzyme in the engaged state (Fig. 3 and Supplementary Fig. 5). This reconstruction shows an additional defined density of appropriate size to accommodate the catalytic domain of Ubp6 or human Usp14 (Fig. 3a). Usp14 and Ubp6 share high structural conservation²³, and we therefore generated a homology model of ubiquitin-bound Ubp6 based on the crystal structure of Usp14–ubiquitin aldehyde (PDB 2AYO²³), which we then docked into the additional electron density of the ATP- γ S-bound proteasome complex. Strikingly, we found that the ubiquitin-bound Ubp6 binds directly to the ATPase hexamer of the base, primarily interacting with Rpt1 (Fig. 3a,e). In the docked model, the N terminus of the ubiquitin-bound catalytic domain is positioned close to the density observed between Ubp6 and Rpn1 (Supplementary Fig. 6); this spanning density is likely to originate from the linker connecting the catalytic domain with the Ubl domain. Ubiquitin-bound Ubp6 contacts the N ring and the AAA+ ring, both of which in the engaged, translocation-competent state of the base are coaxially aligned with the core particle. Ubp6's position at the periphery of the N ring places it directly in front of Rpn11, separated by ~30 Å. Especially in its ubiquitin-bound state, Ubp6 may thus sterically occlude Rpn11's access to ubiquitinated substrates, hence possibly explaining its previously reported inhibitory effects on Rpn11 DUB activity²⁶. Interestingly, this location of the Ubp6 density and its presence in the engaged conformation of the proteasome agree with a previously unspecified density in substrate-processing proteasomes observed by EM tomography of neurons³⁶.

Ubp6 affects proteasomal conformational dynamics

Given the specific interaction of ubiquitin-bound Ubp6 with the ATPase ring in its engaged, translocation-competent conformation, we wanted to characterize Ubp6's effects on substrate degradation

independent of ubiquitin processing. We therefore measured the ubiquitin-independent SspB₂-mediated degradation of a permanently unfolded model substrate as well as a folded GFP model substrate in the presence or absence of Ubp6 (Fig. 4a and Supplementary Data Set 1). In contrast to the previously reported inhibition of ubiquitin-dependent substrate degradation²⁶, ubiquitin-free Ubp6 C118A had minimal effect on ubiquitin-independent degradation. However, Ubp6 C118A bound to diubiquitin inhibited substrate turnover. We observed this inhibition for degradation of both the folded and unfolded substrates, results indicating that ubiquitin-bound Ubp6 does not affect the protein-unfolding abilities of the proteasome. In its ubiquitin-bound state, Ubp6 thus increases the ATPase rate of the base but slows substrate degradation.

One possible explanation for these observations is that Ubp6 stabilizes the engaged, translocation-competent state of the proteasome and inhibits the reversion back to the apo conformation capable of engaging a new substrate. To test this hypothesis, we analyzed degradation of the GFP substrate by SspB₂-fused proteasomes in the presence of ubiquitin-free or ubiquitin-bound Ubp6 under single-turnover conditions (excess enzyme over substrate), under which measured fluorescence signals follow a single-exponential decay (Fig. 4b). Indeed, we observed no effect on single-turnover degradation, consistently with a scenario in which ubiquitin-bound Ubp6 might stabilize but not strongly induce the substrate-engaged state, thus allowing efficient engagement of the first substrate. In contrast, multiple-turnover degradation was strongly inhibited by ubiquitin-bound Ubp6 (Fig. 4c). For degradation in the presence of only diubiquitin or ubiquitin-free Ubp6, the single-turnover rate constants agree well with the k_{cat} values of multiple turnover. These data thus suggest a

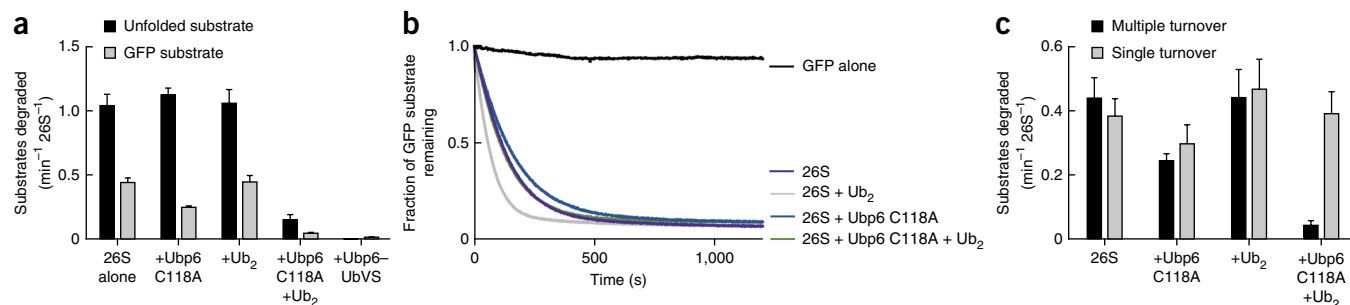


Figure 4 Ubiquitin-bound Ubp6 stabilizes the substrate-engaged conformation of the proteasome, and ubiquitin-independent substrate delivery to the proteasome reveals that ubiquitin-bound Ubp6 allosterically inhibits multiple-turnover but not single-turnover degradation. **(a)** Multiple-turnover degradation of a permanently unfolded model substrate and a GFP-fused substrate by reconstituted SspB₂-Rpt2 proteasomes in the absence or presence of Ubp6 C118A and diubiquitin (Ub₂). Data shown are means and s.e.m. of three technical replicates. Representative gels are shown in **Supplementary Data Set 1**. **(b)** Single-turnover degradation of the GFP-fused substrate by saturating amounts of reconstituted SspB₂-Rpt2 proteasomes in the absence or presence of Ubp6 C118A and Ub₂. Curves shown are representative of three individual experiments. **(c)** Rate constants for degradation of the GFP-fused substrate under multiple- and single-turnover conditions shown in **a** and **b**. Rate constants for single-turnover degradations were determined from a single exponential regression of data; error bars represent s.e.m. of three individual experiments. Compiled experimental data are shown in **Supplementary Data Set 2**.

model in which substrate engagement with the AAA+ ring induces the engaged conformation, which is then stabilized by ubiquitin-bound Ubp6, thus preventing the return to the apo, engagement-competent conformation until ubiquitin dissociates.

Ubp6 inhibition of ubiquitin-dependent degradation

Most substrates are targeted to the proteasome by attached polyubiquitin chains, which must be removed by Rpn11 to allow efficient degradation^{4,5}. We were thus interested in whether the proximity of ubiquitin-bound Ubp6 to Rpn11 inhibited Rpn11-mediated deubiquitination and therefore ubiquitin-dependent substrate degradation. We directly analyzed the deubiquitination activity of Rpn11 by measuring Ub-AMC cleavage of holoenzymes with no Ubp6, Ubp6 C118A, ubiquitin-aldehyde (UbH)-modified wild-type Ubp6 or UbH-modified Ubp6 lacking its N-terminal Ubl domain (**Fig. 5a**). This deubiquitination activity was highly sensitive to the metal

chelator *o*-phenanthroline, thus confirming that it originated from Rpn11 (**Supplementary Fig. 2e**). Covalent modification of Ubp6 with UbH ensured a ubiquitin-bound state without addition of free diubiquitin, which would compete in the Rpn11 Ub-AMC cleavage assay. Ubp6-UbH inhibited Rpn11 by 85%, whereas catalytically inactive Ubp6 C118A showed only 45% inhibition. Ubp6 ΔUbl did not affect Rpn11 activity, thus indicating that the functional interaction with Rpn11 and presumably also binding to the Rpt ring itself depend on the Ubl-mediated tethering of Ubp6 to Rpn11.

As a model substrate for the degradation experiments, we used a lysine-less variant of superfolder GFP³⁷ fused to an unstructured region that contained a single lysine for *in vitro* ubiquitination, thus reducing potential substrate heterogeneity due to multiple chain placements. To ensure a permanently ubiquitin-bound state of Ubp6, we modified its active site with UbVS. Importantly, Ubp6-UbVS behaves similarly to diubiquitin-bound Ubp6, on the basis of stimulation of

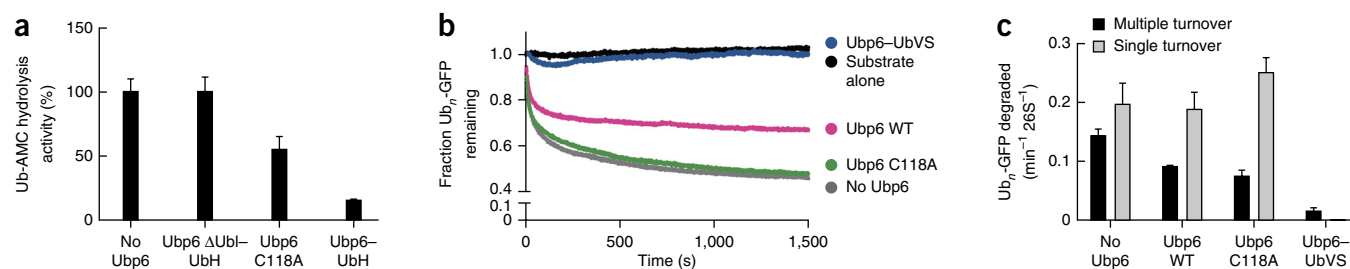


Figure 5 Ubp6 affects ubiquitin-dependent degradation. **(a)** Ubiquitin binding to Ubp6 strongly inhibits Rpn11 deubiquitination activity. Ubp6 (wild type or C118A) was treated with ubiquitin aldehyde (UbH) and added to Ubp6-free holoenzymes purified from yeast. Rpn11 deubiquitination activity was measured by Ub-AMC cleavage. Data are means and s.e.m. of 3 independent experiments. **(b,c)** Effects of Ubp6 on ubiquitin-dependent substrate degradation of the same GFP-fused substrate used for ubiquitin-independent turnover in **Figure 4**, ubiquitinated *in vitro* at an engineered single lysine residue. **(b)** Single-turnover degradation of the polyubiquitinated GFP-fused substrate, measured with saturating amounts of proteasome holoenzyme purified from a Ubp6-knockout yeast strain, with no Ubp6, wild-type Ubp6, Ubp6 C118A or Ubp6-UbVS added back. **(c)** Rate constants for single- and multiple-turnover degradation of the ubiquitinated GFP model substrate. Data shown are means and s.e.m. from three technical replicates. **(d)** Degradation of a polyubiquitinated EGFP^{20,47} substrate, assessed by SDS-PAGE and in-gel GFP fluorescence detection. Proteasomes were purified from ΔUbp6 yeast cells and incubated with buffer or wild-type (WT), C118A or UbVS-treated Ubp6. Compiled experimental data are shown in **Supplementary Data Set 2**.

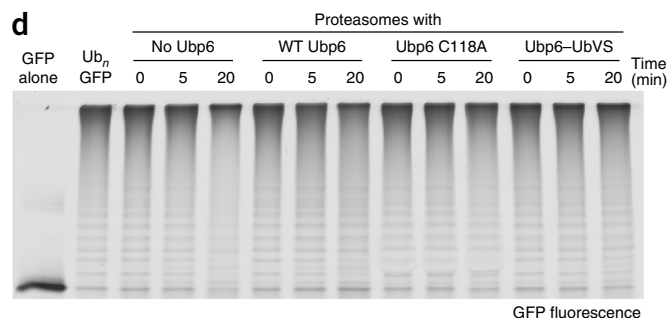
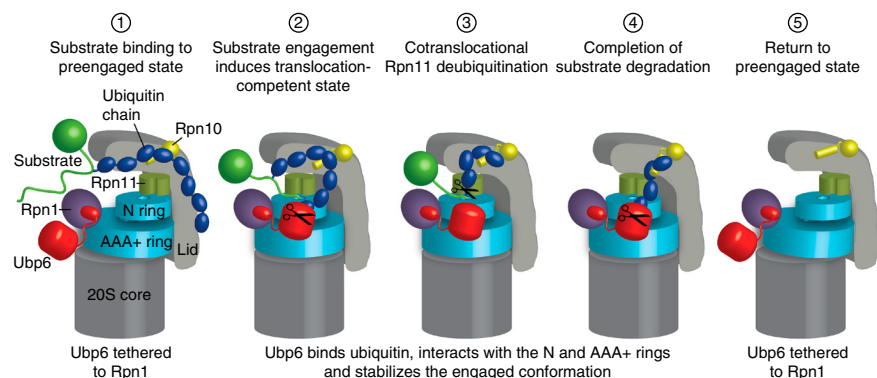


Figure 6 Model for Ubp6 acting as a ubiquitin-dependent timer to allosterically control proteasome conformational changes, Rpn11 deubiquitination and substrate degradation.

(1) Ubiquitin-chain binding to an intrinsic receptor (for example, Rpn10) tethers a substrate to the proteasome. Ubp6 is bound to the proteasome via its Ubl domain interacting with Rpn1. (2) Engagement of the unstructured initiation region of the substrate by the ATPase hexamer induces a conformational switch of the regulatory particle to a substrate-engaged, translocation competent state, characterized by a coaxial alignment of Rpn11, N ring, AAA+ ring and 20S core. If ubiquitin binds, for instance during debranching or trimming of ubiquitin chains, Ubp6 interacts with and stabilizes the engaged state of the ATPase hexamer by bridging the N ring and AAA+ ring. In this state, ubiquitin-bound Ubp6 inhibits Rpn11-mediated deubiquitination and consequently substrate degradation. (3) Translocation moves the ubiquitin-modified lysines of the substrate into the Rpn11 active site for cotranslocational ubiquitin-chain removal. (4) Even after complete substrate translocation, ubiquitin-bound Ubp6 stabilizes the engaged conformation of the proteasome, prevents switching back to the engagement-competent state and thus interferes with the degradation of the subsequent substrate. Such trapping of the engaged state would allow Ubp6 to clear ubiquitin chains from proteasomal receptors before the next substrate is engaged and degradation is initiated. (5) As soon as it is no longer occupied with ubiquitin, the catalytic domain of Ubp6 releases from the N ring and AAA+ ring, and allows the regulatory particle to return to the preengaged state for the next round of substrate degradation.



proteasomal ATP hydrolysis (**Supplementary Fig. 2c**). Substrate degradation was measured under single- and multiple-turnover conditions with proteasomes purified from a Δ Ubp6 yeast strain with added-back wild-type Ubp6, Ubp6 C118A or Ubp6-UbVS (**Fig. 5b,c**). Notably, in contrast to ubiquitin-independent degradation, all ubiquitin-dependent single-turnover traces followed a double-exponential decay, consistently with our previously published data²⁰. We attribute this behavior to potential heterogeneity in the ubiquitin modification of individual substrate molecules, in which shorter ubiquitin chains affect proteasome binding and processing kinetics. In agreement with earlier reports^{26,29}, we observed ~37% slower multiple-turnover degradation in the presence of wild-type Ubp6 and a 48% reduction in rate when the catalytically dead C118A mutant was bound to the proteasome (**Fig. 5c**). Similarly to the results for ubiquitin-independent degradation, there were no substantial defects in single turnover, consistently with our model suggesting that, upon ubiquitin binding, Ubp6 may stabilize the engaged proteasome conformation, prevent switching back to the substrate-free conformation and inhibit engagement of a subsequent substrate for multiple turnover. Proteasomes in complex with Ubp6-UbVS exhibited almost no detectable degradation in both multiple and single turnover (**Fig. 5b,c**).

Finally, gel-based analyses of the processing of an established polyubiquitinated GFP substrate^{18,20} revealed that proteasomes bound to Ubp6-UbVS showed neither substantial degradation nor deubiquitination (**Fig. 5d**). This behavior suggests a model in which permanently ubiquitin-bound Ubp6 binds to the ATPase ring right after the substrate has entered the pore and has induced the engaged conformation. The position of ubiquitin-bound Ubp6 in proximity to Rpn11 may sterically prevent access of Rpn11 to the ubiquitin-modified lysine of our model substrate. Because the proteasome encounters this modified lysine before the GFP moiety, inhibiting ubiquitin-chain removal by Rpn11 would stall translocation and thus prohibit GFP unfolding. However, other substrates may behave differently depending on the substrate geometry and the positions of ubiquitin modifications relative to the degradation-initiation site. In spite of the 45% inhibition of Rpn11 activity by Ubp6 C118A, we did not observe defects in single-turnover substrate degradation for this Ubp6 variant. It is possible that the catalytically inactive Ubp6 C118A is not ubiquitin bound during degradation of the first substrate but holds on to ubiquitin after Rpn11 cleavage, thus affecting

Rpn11 deubiquitination and stabilizing the engaged state in multiple turnover. Alternatively, the on and off rates for uncleaved ubiquitin on Ubp6 C118A may still allow ubiquitin-chain binding and cleavage by Rpn11 but inhibit the base from switching back to the preengaged state for multiple turnover. In a control experiment, we verified that the proteasome did not engage and degrade any of the Ubp6 variants, because this would also inhibit degradation of our model substrate (**Supplementary Fig. 7**).

DISCUSSION

Our biochemical and structural data show that Ubp6, besides having a role in ubiquitin cleavage, affects proteasomal substrate degradation by allosterically interfering with distinct proteasome functions in a ubiquitin-dependent manner. Before substrate engagement by the base, Ubp6 is tethered via its Ubl domain to Rpn1, and its catalytic USP domain appears to be rather mobile, sampling a larger area. Interactions of the USP domain with the base ATPase stimulate deubiquitination activity, probably by changing the conformation of two blocking surface loops in USP, BL1 and BL2 (ref. 23); this activity further increases upon proteasome engagement of a substrate polypeptide. Ubiquitin-bound Ubp6 binds and stabilizes this substrate-engaged, translocation-competent conformation of the proteasome by interacting with both the N ring and the AAA+ ring of the base, thereby maintaining their coaxial alignment with the 20S core. The interaction with the base places ubiquitin-bound Ubp6 in proximity to Rpn11, in a position in which it interferes with Rpn11-mediated substrate deubiquitination. These findings are also consistent with a recent EM structural study³⁸.

Our results suggest a model in which substrate engagement acts as a switch to induce the translocation-competent state of the proteasome, which is then regulated by ubiquitin-bound Ubp6 in two ways: the inhibition of Rpn11 and the interference with conformational switching back to the substrate-free state (**Fig. 6**). Ubp6 would inhibit Rpn11 deubiquitination and therefore slow substrate degradation if it were to interact with ubiquitin before Rpn11 has removed all modifications from the translocating substrate. Such coordination between Ubp6 and Rpn11 activities may be important for complex substrates containing multiple, very long or branched polyubiquitin chains that need to be cotranslocationally trimmed by Ubp6. After Rpn11 has cleaved off all ubiquitin modifications, and the substrate has been

completely unfolded and translocated, Ubp6 may trap the engaged conformation of the proteasome and prevent the engagement of a subsequent substrate until it is no longer occupied with ubiquitin. This mechanism may be important for Ubp6-mediated clearance of polyubiquitin chains from the ubiquitin receptors before the proteasome commits to the degradation of a new substrate, and it would be concordant with Ubp6's role in maintaining high levels of free ubiquitin in the cell^{39,40}.

In our studies, we either saturated ubiquitin binding to catalytically dead Ubp6 or used covalent ubiquitin fusions to exaggerate the effects on proteasomal functions. However, given the fast kinetics of ubiquitin cleavage by Ubp6 compared to Rpn11, wild-type Ubp6 that is processing ubiquitin modifications would not be expected to severely slow proteasomal substrate degradation. Ubp6 may instead act as a timer, not only as previously suggested by trimming ubiquitin chains and thus affecting the persistence time of substrates at the proteasome but also in a ubiquitin-dependent manner by allosterically coordinating the various substrate-processing steps at the proteasome and preventing stalling of substrates with complex ubiquitin modifications.

Our EM structural work provides what is to our knowledge the first visualization of ubiquitin-bound Ubp6 in the context of the 26S proteasome. Future higher-resolution structures will be needed to elucidate the detailed mechanisms involved in the reciprocal stimulation of Ubp6 deubiquitination and base ATPase activities. It will also be interesting to investigate how Ubp6 coordinates with other proteasome-bound cofactors, for instance the ubiquitin ligase Hul5 (refs. 24,41,42) or ubiquitin shuttle receptors Rad23, Ddi1 and Dsk2 (refs. 15,25,43,44), in fine-tuning substrate processing by the 26S proteasome.

METHODS

Methods and any associated references are available in the [online version of the paper](#).

Accession codes. The EM density maps for the 26S proteasomes in the presence and absence of ubiquitin-bound Ubp6 have been deposited in the the Electron Microscopy Data Bank under accession numbers EMD-2995 and EMD-6334, respectively.

Note: Any Supplementary Information and Source Data files are available in the [online version of the paper](#).

ACKNOWLEDGMENTS

We thank the members of the Martin laboratory for helpful discussions, C. Padovani and R. Beckwith (both in A.M.'s laboratory) for purified ubiquitin dimers and proteasome base subcomplexes, respectively. We are also grateful to T. Wandless (Stanford School of Medicine) for providing the lysineless GFP construct, K. Nyquist for cloning the GFP model substrate used in degradation assays and the D.O. Morgan laboratory (University of California, San Francisco) for ubiquitin reagents. C.B. acknowledges support from the US National Science Foundation Graduate Research Fellowship, and M.E.M. acknowledges support from the American Cancer Society (grant 121453-PF-11-178-01-TBE). This research was also funded in part by the Damon Runyon Cancer Research Foundation (DFS-#07-13), the Pew Scholars program, the Searle Scholars program and the US National Institutes of Health (grant DP2 EB020402-01) to G.C.L. A.M. acknowledges support from the Searle Scholars Program, start-up funds from the Molecular & Cell Biology Department at the University of California, Berkeley, the US National Institutes of Health (grant R01-GM094497) and the US National Science Foundation CAREER Program (NSF-MCB-1150288).

AUTHOR CONTRIBUTIONS

C.B., E.A.G., M.E.M. and A.M. designed, expressed, and purified proteasome components and performed biochemical experiments. C.M.D. and G.C.L. performed EM, data processing and segmentation analyses. All authors contributed to experimental design, data analyses and manuscript preparation.

COMPETING FINANCIAL INTERESTS

The authors declare no competing financial interests.

Reprints and permissions information is available online at <http://www.nature.com/reprints/index.html>.

1. Finley, D. Recognition and processing of ubiquitin-protein conjugates by the proteasome. *Annu. Rev. Biochem.* **78**, 477–513 (2009).
2. Goldberg, A.L. Protein degradation and protection against misfolded or damaged proteins. *Nature* **426**, 895–899 (2003).
3. Goldberg, A.L. Functions of the proteasome: from protein degradation and immune surveillance to cancer therapy. *Biochem. Soc. Trans.* **35**, 12–17 (2007).
4. Verma, R. *et al.* Role of Rpn11 metalloprotease in deubiquitination and degradation by the 26S proteasome. *Science* **298**, 611–615 (2002).
5. Yao, T. & Cohen, R.E. A cryptic protease couples deubiquitination and degradation by the proteasome. *Nature* **419**, 403–407 (2002).
6. Groll, M. *et al.* Structure of 20S proteasome from yeast at 2.4 Å resolution. *Nature* **386**, 463–471 (1997).
7. Martin, A., Baker, T.A. & Sauer, R.T. Pore loops of the AAA+ ClpX machine grip substrates to drive translocation and unfolding. *Nat. Struct. Mol. Biol.* **15**, 1147–1151 (2008).
8. Maillard, R.A. *et al.* ClpX(P) generates mechanical force to unfold and translocate its protein substrates. *Cell* **145**, 459–469 (2011).
9. Aubin-Tam, M.-E., Olivares, A.O., Sauer, R.T., Baker, T.A. & Lang, M.J. Single-molecule protein unfolding and translocation by an ATP-fueled proteolytic machine. *Cell* **145**, 257–267 (2011).
10. Xu, P. *et al.* Quantitative proteomics reveals the function of unconventional ubiquitin chains in proteasomal degradation. *Cell* **137**, 133–145 (2009).
11. Kim, W. *et al.* Systematic and quantitative assessment of the ubiquitin-modified proteome. *Mol. Cell* **44**, 325–340 (2011).
12. Saeki, Y. *et al.* Lysine 63-linked polyubiquitin chain may serve as a targeting signal for the 26S proteasome. *EMBO J.* **28**, 359–371 (2009).
13. Zhang, N. *et al.* Structure of the s5a:k48-linked diubiquitin complex and its interactions with rpn13. *Mol. Cell* **35**, 280–290 (2009).
14. Riedinger, C. *et al.* Structure of Rpn10 and its interactions with polyubiquitin chains and the proteasome subunit Rpn12. *J. Biol. Chem.* **285**, 33992–34003 (2010).
15. Elsasser, S., Chandler-Millitello, D., Müller, B., Hanna, J. & Finley, D. Rad23 and Rpn10 serve as alternative ubiquitin receptors for the proteasome. *J. Biol. Chem.* **279**, 26817–26822 (2004).
16. Zhang, D. *et al.* Together, Rpn10 and Dsk2 can serve as a polyubiquitin chain-length sensor. *Mol. Cell* **36**, 1018–1033 (2009).
17. Mayor, T., Graumann, J., Bryan, J., MacCoss, M.J. & Deshaies, R.J. Quantitative profiling of ubiquitylated proteins reveals proteasome substrates and the substrate repertoire influenced by the Rpn10 receptor pathway. *Mol. Cell. Proteomics* **6**, 1885–1895 (2007).
18. Lander, G.C. *et al.* Complete subunit architecture of the proteasome regulatory particle. *Nature* **482**, 186–191 (2012).
19. Beck, F. *et al.* Near-atomic resolution structural model of the yeast 26S proteasome. *Proc. Natl. Acad. Sci. USA* **109**, 14870–14875 (2012).
20. Beckwith, R., Estrin, E., Worden, E.J. & Martin, A. Reconstitution of the 26S proteasome reveals functional asymmetries in its AAA+ unfoldase. *Nat. Struct. Mol. Biol.* **20**, 1164–1172 (2013).
21. Matyskiela, M.E., Lander, G.C. & Martin, A. Conformational switching of the 26S proteasome enables substrate degradation. *Nat. Struct. Mol. Biol.* **20**, 781–788 (2013).
22. Śledź, P. & Unverdorben, P. Structure of the 26S proteasome with ATP-γS bound provides insights into the mechanism of nucleotide-dependent substrate translocation. *Proc. Natl. Acad. Sci. USA* **110**, 7264–7269 (2013).
23. Hu, M. *et al.* Structure and mechanisms of the proteasome-associated deubiquitinating enzyme USP14. *EMBO J.* **24**, 3747–3756 (2005).
24. Leggett, D.S. *et al.* Multiple associated proteins regulate proteasome structure and function. *Mol. Cell* **10**, 495–507 (2002).
25. Elsasser, S. *et al.* Proteasome subunit Rpn1 binds ubiquitin-like protein domains. *Nat. Cell Biol.* **4**, 725–730 (2002).
26. Hanna, J. *et al.* Deubiquitinating enzyme Ubp6 functions noncatalytically to delay proteasomal degradation. *Cell* **127**, 99–111 (2006).
27. Peth, A., Besche, H.C. & Goldberg, A.L. Ubiquitinated proteins activate the proteasome by binding to Usp14/Ubp6, which causes 20S gate opening. *Mol. Cell* **36**, 794–804 (2009).
28. Peth, A., Kukushkin, N., Bossé, M. & Goldberg, A.L. Ubiquitinated proteins activate the proteasomal ATPases by binding to Usp14 or Uch37 homologs. *J. Biol. Chem.* **288**, 7781–7790 (2013).
29. Lee, B.-H. *et al.* Enhancement of proteasome activity by a small-molecule inhibitor of USP14. *Nature* **467**, 179–184 (2010).
30. Torres, E.M. *et al.* Identification of aneuploidy-tolerating mutations. *Cell* **143**, 71–83 (2010).
31. Dephoure, N. *et al.* Quantitative proteomic analysis reveals posttranslational responses to aneuploidy in yeast. *eLife* **3**, e03023 (2014).
32. Walters, B.J. *et al.* A catalytic independent function of the deubiquitinating enzyme USP14 regulates hippocampal synaptic short-term plasticity and vesicle number. *J. Physiol. (Lond.)* **592**, 571–586 (2014).
33. Levchenko, I. A specificity-enhancing factor for the ClpXP degradation machine. *Science* **289**, 2354–2356 (2000).



34. Dong, K.C. *et al.* Preparation of distinct ubiquitin chain reagents of high purity and yield. *Structure* **19**, 1053–1063 (2011).
35. Borodovsky, A. *et al.* A novel active site-directed probe specific for deubiquitylating enzymes reveals proteasome association of USP14. *EMBO J.* **20**, 5187–5196 (2001).
36. Asano, S. *et al.* A molecular census of 26S proteasomes in intact neurons. *Science* **347**, 439–442 (2015).
37. Chu, B.W. *et al.* The E3 ubiquitin ligase UBE3C enhances proteasome processivity by ubiquitinating partially proteolyzed substrates. *J. Biol. Chem.* **288**, 34575–34587 (2013).
38. Aufderheide, A. *et al.* Structural characterization of the interaction of Ubp6 with the 26S proteasome. *Proc. Natl. Acad. Sci. USA* **112**, 8626–8631 (2015).
39. Marshall, A.G. *et al.* Genetic background alters the severity and onset of neuromuscular disease caused by the loss of ubiquitin-specific protease 14 (Usp14). *PLoS ONE* **8**, e84042 (2013).
40. Chen, P.-C. *et al.* The proteasome-associated deubiquitinating enzyme Usp14 is essential for the maintenance of synaptic ubiquitin levels and the development of neuromuscular junctions. *J. Neurosci.* **29**, 10909–10919 (2009).
41. Crosas, B. *et al.* Ubiquitin chains are remodeled at the proteasome by opposing ubiquitin ligase and deubiquitinating activities. *Cell* **127**, 1401–1413 (2006).
42. Aviram, S. & Kornitzer, D. The ubiquitin ligase Hul5 promotes proteasomal processivity. *Mol. Cell. Biol.* **30**, 985–994 (2010).
43. Inobe, T., Fishbain, S., Prakash, S. & Matouschek, A. Defining the geometry of the two-component proteasome degron. *Nat. Chem. Biol.* **7**, 161–167 (2011).
44. Gomez, T.A., Kolawa, N., Gee, M., Sweredoski, M.J. & Deshaies, R.J. Identification of a functional docking site in the Rpn1 LRR domain for the UBA-UBL domain protein Ddi1. *BMC Biol.* **9**, 33 (2011).
45. Unverdorben, P. *et al.* Deep classification of a large cryo-EM dataset defines the conformational landscape of the 26S proteasome. *Proc. Natl. Acad. Sci. USA* **111**, 5544–5549 (2014).
46. Worden, E.J., Padovani, C. & Martin, A. Structure of the Rpn11–Rpn8 dimer reveals mechanisms of substrate deubiquitination during proteasomal degradation. *Nat. Struct. Mol. Biol.* **21**, 220–227 (2014).
47. Lander, G.C. *et al.* Appion: an integrated, database-driven pipeline to facilitate EM image processing. *J. Struct. Biol.* **166**, 95–102 (2009).

ONLINE METHODS

Yeast strains. Yeast lid and holoenzyme were purified from strain YYS40 (genotype *MATa ade2-1 his3-11,15 leu2-3,112 trp1-1 ura3-1 can1 Rpn11::Rpn11-3×Flag(His₃)*)⁴⁸. Core particles were prepared from either strain RJD1144 (genotype *MATa his3Δ200 leu2-3,112 lys2-801 trpΔ63 ura3-52 PRE1-Flag-His₃::Ylpac211(URA3)*)⁴⁹ or strain yAM14 (genotype *MATa ade2-1 his3-11,15 leu2-3,112 trp1-1 ura3-1 can1-100 bar1 PRE1::PRE1-3×Flag(KanMX)*)²⁰. To generate *UBP6*-deletion strains, the *kanMX6* sequence was integrated at the relevant genomic locus, replacing the gene in YYS40 (ref. 18). To generate the *UBP6* C118A strain, a C118A copy of *Ubp6* was cloned into pRS305 and was integrated into the *UBP6*-deletion strain at the *leu2* locus.

Purification of yeast holoenzyme and subcomplexes. Wild-type and mutant proteasome were purified from *S. cerevisiae* essentially as previously described^{18,21}. In summary, holoenzyme, lid, and core particle were purified from yeast strains listed above. Lysed cells were resuspended in lysis buffer containing 60 mM HEPES, pH 7.6, 50 mM NaCl, 50 mM KCl, 5 mM MgCl₂, 0.5 mM EDTA, 10% glycerol, and 0.2% NP-40. Holoenzyme lysis also included an ATP-regeneration mix (5 mM ATP, 0.03 mg/ml creatine kinase and 16 mM creatine phosphate). Complexes were bound to anti-Flag M2 affinity resin (Sigma) and washed with wash buffer (60 mM HEPES, pH 7.6, 50 mM NaCl, 50 mM KCl, 5 mM MgCl₂, 0.5 mM EDTA, 10% glycerol, 0.1% NP-40 and 500 mM ATP). Core particles were washed with wash buffer containing 500 mM NaCl, and lids were washed with wash buffer containing 1 M NaCl. Complexes were eluted with Flag peptide and separated by size-exclusion chromatography over Superose-6 in gel-filtration (GF) buffer (60 mM HEPES, pH 7.6, 50 mM NaCl, 50 mM KCl, 5 mM MgCl₂, 0.5 mM EDTA and 0.5 mM ATP) containing 5% glycerol.

Recombinant expression and purification of proteins and complexes. Base subcomplexes were expressed and purified from *E. coli* as previously described²⁰. Nine integral subunits (Rpn1, Rpn2, Rpn13, and Rpts 1–6) and four assembly chaperones (Rpn14, Hsm3, Nas2, and Nas6) were expressed with rare tRNAs overnight at 18 °C after induction with 0.5 mM IPTG. Cells were harvested by centrifugation and resuspended in nickel buffer (60 mM HEPES, pH 7.6, 100 mM NaCl, 100 mM KCl, 10% glycerol, 10 mM MgCl₂, 0.5 mM EDTA, and 20 mM imidazole) supplemented with 2 mg ml⁻¹ lysozyme, protease inhibitors (aprotinin, pepstatin, leupeptin, and PMSF) and benzonase (Novagen). Cells were lysed by freeze-thaw cycles and sonication and clarified by centrifugation. A two-step affinity purification of the base subcomplex was performed with nickel–nitrilotriacetic acid (Ni-NTA) agarose (Qiagen) to select for His₆-Rpt3 and with anti-Flag M2 resin (Sigma-Aldrich) to select for Flag-Rpt1. 0.5 mM ATP was present in all purification buffers. The Ni-NTA and anti-Flag M2 columns were eluted with nickel buffer containing 250 mM imidazole and 0.15 mg ml⁻¹ 3×Flag peptide, respectively. The Flag-column eluate was concentrated and run on a Superose 6 size-exclusion column (GE Healthcare) equilibrated with gel-filtration buffer (60 mM HEPES, pH 7.6, 50 mM NaCl, 50 mM KCl, 10% glycerol, 5 mM MgCl₂, 0.5 mM EDTA, 1 mM DTT, and 0.5 mM ATP).

The GFP-fused substrate construct was cloned into a pET Duet (Novagen) vector, and it consisted of a lysineless superfolder GFP³⁷, a lysineless titin I27 V15P domain, and a random coil containing the *ssrA* sequence and the PPTY motif. *E. coli* BL21 Star (DE3) cells were transformed with the construct and grown in Terrific Broth (EMD Millipore) at 30 °C. Cells were induced with 0.5 mM IPTG at an OD₆₀₀ of 1–1.5, and expression continued for 5 h at 30 °C.

The unfolded substrate was cloned into a pET 28A (Novagen) vector, and it consisted of a lysineless, disulfideless N1 domain from gene-3-protein⁵⁰ fused to a random coil containing an *ssrA* tag, ppxy motif, and a lysineless StrepII tag. WT *Ubp6* was amplified from genomic (W303) DNA, and cloned into pET Duet with an N-terminal His₆ tag. C118A mutation was made by around-the-horn PCR. *E. coli* BL21 Star (DE3) cells were transformed with either the N1 construct or the *Ubp6* constructs and grown in Terrific Broth at 37 °C. Cells were induced with 0.5 mM IPTG at an OD₆₀₀ of 0.6, and expression continued overnight at 18 °C.

GFP-, unfolded substrate-, or *Ubp6*-expressing cells were harvested by centrifugation and resuspended in nickel buffer (above) supplemented with 2 mg ml⁻¹ lysozyme, benzonase (Novagen), and protease inhibitors (aprotinin, pepstatin, leupeptin and PMSF). Cells were lysed by freeze thaw and sonication. Lysates were clarified by centrifugation at 15,000 r.p.m. for 20 min at 4 °C. Proteins were purified by Ni-NTA affinity chromatography followed by size-exclusion

chromatography on a Superdex 200 (GE Healthcare) with nickel and gel-filtration buffers mentioned above.

Construction of the SspB₂ permutant base. To allow ubiquitin-independent substrate delivery to the proteasome, we created a base variant fused to a linked permutant dimer of the *E. coli* substrate adaptor SspB. A wild-type SspB monomer consists of a globular domain and a C-terminal tail of 38 residues. In simple dimer fusions, in which we connected the C terminus of the globular domain of one SspB monomer with the N terminus of the second SspB monomer, the linker interfered with *ssrA* substrate binding to SspB₂. We therefore constructed a circular permutant SspB monomer, in which we created a new N terminus at residue L26, connected the preceding N-terminal helix to the C terminus of the globular domain, and fused this monomer to the N terminus of a second wild-type SspB monomer. The connectivity of this covalently fused dimer is (L26-D111)-GGASG-(S4-Q25)-GGGTGG-(wild-type monomer). This SspB₂ dimer was then fused to the N terminus of Rpt2 of the base.

Ubiquitin purification and dimer synthesis. Ubiquitin was expressed and purified as previously described^{46,51}. Briefly, Rosetta II (DE3) pLysS *E. coli* cells were transformed with a pET28a vector containing the ubiquitin gene from *S. cerevisiae* under control of a T7 promoter. Cells were grown in Terrific Broth supplemented with 1% glycerol at 37 °C until the OD₆₀₀ reached 1.5–2.0 and were induced with 0.5 mM IPTG overnight at 18 °C. The lysis buffer contained 50 mM Tris-HCl, pH 7.6, 0.02% NP-40, 2 mg ml⁻¹ lysozyme, benzonase (Novagen), and protease inhibitors (aprotinin, pepstatin, leupeptin and PMSF). Cells were lysed by sonication and 20-min incubation at room temperature. Lysate was clarified by centrifugation at 15,000 r.p.m. Clarified lysate was precipitated by addition of 60% perchloric acid to a final concentration of 0.5%, and the solution was stirred on ice for a total of 20 min. A 5-ml HiTrap SP FF column (GE Life Sciences) was used for cation-exchange chromatography, and ubiquitin fractions were pooled and exchanged into Ub storage buffer (20 mM Tris-HCl, pH 7.6, and 150 mM NaCl) by repeated dilution and concentration. K48-ubiquitin dimers were synthesized and purified as previously described³⁴.

Preparation of ubiquitin-fused Ubp6. 50 μM WT *Ubp6* or Δ*Ubl* *Ubp6* protein was reacted with 75 μM ubiquitin vinyl sulfone or ubiquitin aldehyde (R&D Systems) in GF buffer at 37 °C. For the experiment in Figure 5d, which required complete inhibition of the active site cysteine, buffer, wild-type *Ubp6*, or C118A *Ubp6* was reacted with ubiquitin aldehyde for 7 h at 37 °C in the dark. To ensure complete inactivation, *Ubp6*-UbH was further reacted with 500 μM NEM for 30 min at 30 °C; this was followed by quenching with 5 mM DTT for another 30 min at 30 °C. Ubiquitin aldehyde, NEM, and DTT were removed by dilution and concentration in an Amicon 30K-MWCO concentrator (EMD Millipore).

Ubiquitin-AMC hydrolysis assays. Ubiquitin-AMC (R&D Systems) hydrolysis was measured in a QuantaMaster spectrofluorimeter (PTI) by monitoring an increase of fluorescence emission at 435 nm with an excitation at 380 nm. Reactions with reconstituted proteasome contained 100 nM *Ubp6*, 150 nM Rpn1, 150 nM recombinant base, 300 nM CP, 300 nM lid, 300 nM Rpn10, 20 μM unfolded substrate, and 3–10 μM Ub-AMC. Reactions with proteasomes purified from yeast contained 100 nM proteasome. Reactions were carried out either in the presence GF buffer (described above) with 1 mM DTT and 1× ATP-regeneration system or 1 mM ATP-γS. Samples were incubated at 30 °C for 5–10 min before the addition of substrate to ensure *Ubp6* association and nucleotide exchange.

ATPase assays. ATPase activity was quantified by an NADH-coupled ATPase assay. Reconstituted proteasomes (200 nM base, 600 nM core, 600 nM lid, and 600 nM Rpn10), *Ubp6*, (200 nM) Ub₂^{K48} (20 μM), and unfolded gene-3-protein substrate (20 μM) were incubated with 1× ATPase mix (3 U ml⁻¹ pyruvate kinase, 3 U ml⁻¹ lactate dehydrogenase, 1 mM NADH, and 7.5 mM phosphoenolpyruvate) at 30 °C. Reactions were performed in GF buffer (described above) with 1 mM DTT. Absorbance at 340 nm was monitored at 30 °C for 600 s at 1-s intervals by a UV-vis spectrophotometer (Agilent).

Multiple- and single-turnover ubiquitin-independent degradation assays. 26S proteasomes were reconstituted with recombinant, heterologously expressed SspB₂-Rpt2 base, recombinant Rpn10, and lid and core subcomplexes purified

from yeast. Multiple-turnover degradations were performed with 200 nM CP, 600 nM lid, 600 nM base, 600 nM Rpn10, 900 nM Ubp6, and 20 μM Ub₂^{K48}. Reactions were carried out in the presence of 1 \times ATP-regeneration system (5 mM ATP, 0.03 mg ml⁻¹ creatine kinase, and 16 mM creatine phosphate) in gel-filtration buffer with 1 mM DTT. Single-turnover reactions were carried out with 3 μM SspB₂-Rpt2 base, 4.5 μM lid, 4.5 μM base, 4.5 μM Rpn10, 9 μM Ubp6, 20 μM Ub₂^{K48}, and 300 nM substrate in the presence of 1 \times ATP-regeneration system in gel-filtration buffer with DTT and ATP-regeneration system. GFP single- and multiple-turnover degradation activities were monitored by the loss of GFP fluorescence (excitation, 467 nm; emission, 511 nm) with a QuantaMaster spectrofluorimeter (PTI). Single-turnover curves were fit to a single exponential in GraphPad Prism 6.

To track degradation of an unfolded substrate, purified N1 fusion substrates were labeled on a single cysteine with Alexa 647 maleimide at pH 7.2 for 3 h at room temperature in the dark, before quenching of unreacted dye with DTT. Free dye was removed on a Superdex 200 column. Substrate degradation was measured at various time points of reactions at 30 °C and was assessed by SDS-PAGE and subsequent imaging on a Typhoon Trio (GE) with a 633-nm laser and 670-nm BP emission filter. Band intensity was quantified with Image Quant software. Degradation reactions consisted of 8 μM substrate against proteasomes reconstituted as above with either SspB₂-Rpt2 base or WT base to correct for any nonspecific, SspB₂-independent substrate cleavage.

Preparation of ubiquitinated substrates. GFP substrates (20 μM) were modified with polyubiquitin chains by 5 μM yeast Uba1, 5 μM yeast Ubc1, 5 μM Rsp5, 1 \times ATP-regeneration system, and 300 μM ubiquitin. Reactions were carried out in a thermocycler for 2 h at 25 °C, then overnight at 4 °C.

Multiple- and single-turnover ubiquitin-dependent degradation assays. GFP constructs were ubiquitinated overnight and then used the next day without freezing. Single- and multiple-turnover degradation activities were monitored by the loss of GFP fluorescence (excitation, 467 nm; emission, 511 nm) with a QuantaMaster spectrofluorimeter (PTI) as described above. Multiple-turnover reactions consisted of 300 nM purified proteasomes from a ΔUbp6 strain, 600 nM Ubp6, and 2 μM substrate. Single-turnover reactions consisted of 3 μM proteasome, 6 μM Ubp6, and 300 nM substrate.

For the gel-based assessment of substrate degradation and deubiquitination, 2 μM ubiquitinated EGFP substrate was incubated with 200 nM ΔUbp6 proteasomes in the presence of buffer or 400 nM WT, C118A or UbVS-treated Ubp6. Aliquots at different time points were separated on an SDS-PAGE gel, and the gel was imaged on a Typhoon Trio (GE) with excitation at 488 nm and a 526-nm SP emission filter.

Electron microscopy. Samples of 26S-bound Ubp6-UbVS were diluted to ~25 nM in 60 mM HEPES, pH 7.6, 50 mM NaCl, 50 mM KCl, 5 mM MgCl₂, 0.5 mM EDTA, 1 mM TCEP and either 1 mM ATP or 1 mM ATP- γS (Sigma). A thin layer of carbon was applied to 400-mesh Cu-Rh maxtaform grids (Electron Microscopy Sciences) by chemical-vapor deposition, and grids were subsequently exposed to a 95% Ar/5% O₂ plasma for 20 s to glow-discharge/activate the carbon surface. Grids were pretreated with 4 μl of 0.1% poly-L-lysine hydrobromide (Polysciences) to prevent preferred orientation of 26S particles on carbon. Poly-L-lysine solution was then wicked away, grids were washed with 4 μl of H₂O, and 4 μl of sample was applied. 252 and 357 images of negatively stained (2% uranyl formate) 26S-Ubp6-UbVS complexes in the presence of ATP or ATP- γS ,

respectively, were collected at a nominal magnification of 52,000 \times on an F416 CMOS 4,000 \times 4,000 camera (TVIPS) with a pixel size of 2.05 Å/pixel at the sample level. Images were acquired on a Tecnai Spirit LaB₆ electron microscope operating at 120 keV, with a random defocus range of -0.5 μm to -1.5 μm and an electron dose of 20e⁻/Å². Data were acquired with the Legion automated image-acquisition software⁵².

Processing. All image preprocessing and 2D analysis were performed with the Appion image-processing pipeline⁴⁷. CTF was estimated with CTFIND3, and only micrographs having a CTF confidence greater than 80% were used for processing. Particle picking was performed with the template-based FindEM software⁵³. Micrographs were phase-flipped with EMAN's 'applyctf' function, and particles were extracted with a box size of 384 pixels. Pixel values 4.5 σ above or below the mean were replaced with the mean intensity of the extracted particle with XMIPP. Multiple rounds of iterative MSA/MRA were used for 2D classification and alignment of the particles, and class averages containing single-capped proteasomes, as well as damaged, aggregated, or false particles, were removed, thus resulting in a data set containing 24,411 and 18,565 double-capped proteasome particles in the presence of 1 mM ATP and 1 mM ATP- γS , respectively. 3D classification and 3D refinement were performed with C2 symmetry imposed in RELION v1.31 (ref. 54). The 3D reconstructions for proteasomes in the presence of ATP and ATP- γS resolved to 24.2 Å and 22.3 Å, respectively, according to a gold-standard Fourier shell correlation at 0.143. Low-resolution intensities were dampened with a SPIDER script to allow clearer visualization of domain features.

3D modeling. An atomic model of yeast Ub-bound Ubp6 was constructed by superimposing the yeast Ubp6 crystal structure (PDB 1VJV) onto the structure of human Rsp14 bound to ubiquitin (PDB 2AYO)²³, with UCSF Chimera's MatchMaker tool. These structures have high structural homology, and the resulting hybrid structure did not exhibit any clashes between the ubiquitin and Ubp6. This Ubp6-Ub model was docked into the density putatively corresponding to Ubp6. PDB 4CR4 (ref. 45) was used for docking other 26S core, base and lid subunits into the ATP- γS electron density map obtained here, with the exception of the Rpn8-Rpn11 dimer, for which PDB 4O8Y⁴⁶ was used. All docking of PDB structures was performed with the Fit in Map tool of UCSF Chimera, and this software was also used to generate all figures displaying the EM density⁵⁵.

48. Saeki, Y., Isono, E. & Toh, E.A. Preparation of ubiquitinated substrates by the PY motif-insertion method for monitoring 26S proteasome activity. *Methods Enzymol.* **399**, 215–227 (2005).
49. Verma, R. *et al.* Proteasomal proteomics: identification of nucleotide-sensitive proteasome-interacting proteins by mass spectrometric analysis of affinity-purified proteasomes. *Mol. Biol. Cell* **11**, 3425–3439 (2000).
50. Kather, I., Bippes, C.A. & Schmid, F.X. A stable disulfide-free gene-3-protein of phage fd generated by *in vitro* evolution. *J. Mol. Biol.* **354**, 666–678 (2005).
51. Pickart, C.M. & Raasi, S. Controlled synthesis of polyubiquitin chains. *Methods Enzymol.* **399**, 21–36 (2005).
52. Carragher, B. *et al.* Legion: an automated system for acquisition of images from vitreous ice specimens. *J. Struct. Biol.* **132**, 33–45 (2000).
53. Roseman, A.M. FindEM: a fast, efficient program for automatic selection of particles from electron micrographs. *J. Struct. Biol.* **145**, 91–99 (2004).
54. Scheres, S.H.W. RELION: implementation of a Bayesian approach to cryo-EM structure determination. *J. Struct. Biol.* **180**, 519–530 (2012).
55. Goddard, T.D., Huang, C.C. & Ferrin, T.E. Visualizing density maps with UCSF Chimera. *J. Struct. Biol.* **157**, 281–287 (2007).